FT-IR Microspectroscopy Enhances Biological and Ecological Analysis of Algae

Justin N. Murdock [a]; David L. Wetzel [b]

[a] Division of Biology, Kansas State University, Manhattan, Kansas [b] Microbeam Molecular Spectroscopy
Laboratory, Kansas State University, Manhattan, Kansas

Online Publication Date: 01 July 2009

PLEASE SCROLL DOWN FOR ARTICLE

Taylor & Francis
Taylor & Francis Group

FT-IR Microspectroscopy Enhances Biological and Ecological Analysis of Algae

Justin N. Murdock[1] and David L. Wetzel[2]

[1]Division of Biology, Kansas State University, Manhattan, Kansas
[2]Microbeam Molecular Spectroscopy Laboratory, Kansas State University,
Manhattan, Kansas

Abstract: Fourier Transform Infrared (FT-IR) microspectroscopy provides an in situ, nondestructive chemical analysis of individual algal cells. Algae play key roles in nutrient cycling and energy flow through aquatic ecosystems and are pivotal in the sequestration of inorganic nutrients (e.g., carbon, nitrogen, and phosphorus) and transformation into organic forms. However, most methods used to measure algal nutritional and physiological changes are limited to detecting whole community responses because of the relatively large quantity of material needed for analysis (i.e., milligrams to grams). The spatial resolution achievable with infrared microspectroscopy allows for the analysis of macromolecular pools (e.g., proteins, lipids, carbohydrates) in individual cells that allows species specific measurements within heterogeneous microscopic communities. Initial applications characterized molecular pools within marine macroalgae and have since progressed toward ecologically based questions concerning algal physiological responses to changing nutrient availability in marine and freshwater ecosystems.

Keywords: Infrared microspectroscopy, imaging, microbes, periphyton, phytoplankton, synchrotron

INTRODUCTION

Understanding how algal assemblages change with shifting environmental conditions is becoming increasingly important because of their ability to mitigate

aquatic pollution and increasing negative impacts associated with algal blooms. Algae are a fundamental component of most aquatic ecosystems and serve as the energy base of most freshwater and marine food webs. Algae play key roles in nutrient cycling and energy flow through these systems because they are pivotal in the sequestration of inorganic nutrients (e.g., carbon [C], nitrogen [N], and phosphorus [P]) and transformation of nutrients into organic forms (1, 2).

Increased nutrient inputs into lakes, streams, and estuaries by humans typically leads to increased algal biomass and productivity and shifted species composition (3, 4). Algal blooms can decrease dissolved oxygen levels as they respire and decompose or release toxins, causing fish kills. Additionally, algal blooms in water bodies providing drinking water can cost municipalities millions of dollars to mitigate associated taste and odor problems, and decreased water clarity and aesthetics can lower shoreline property values (5). On the other hand, algae are becoming a focus of biotechnological research and application. For example, algae can be used in municipal wastewater treatment to remove nutrients from effluent (6, 7). Methods are currently being developed to use algae to sequester carbon dioxide from coal-fired power plants to aid in mitigating anthropogenic increases in atmospheric carbon dioxide concentrations (8–10). There is also renewed interest in algal use as a biodiesel feedstock for automobile and jet engine fuel.

Traditional methods (e.g., light microscopy) can identify the shifts in algal assemblage composition and abundance due to external cues. These measurements elucidate the final outcomes of species composition changes, but they do not reveal the mechanisms (i.e., cellular physiological response) that produce ending communities. Algal physiological changes such as nutrient content or uptake kinetics from natural assemblages are often limited to whole assemblage responses and often include non-algal components. Limited knowledge of species-specific physiological responses limits the ability to predict community-level functional changes, such as nutrient sequestration or toxin production, with changing environmental conditions. Vibrational spectroscopy provides a means to measure differences in specific chemicals within individual algal cells.

Vibrational spectroscopy on a macroscale, including Fourier Transform Infrared (FT-IR), has been widely used to study the chemical composition of biological material. Since the development of the first research-grade infrared (IR) confocal microscope (11), which was designed for forensic and materials science, infrared microspectroscopy (IMS) has extended the application of vibrational spectroscopy to biological analysis including plant (12, 13) and mammalian tissue (14, 15). Concerning algae, IMS spatial resolution provides single-cell, and thus species-specific, analysis in mixed species microbial communities. Also, synchrotron IMS increases spatial resolution and allows the analysis of smaller species and better subcellular localization of macromolecules (16). There has been a progression of algal IMS research from a strictly biological focus concerning the identification and location of

cellular contents to an ecological focus of species-specific or multispecies response to environmental changes. This review summarizes algal IMS research to date, including algal macromolecular pools of interest and the applications and questions that have been addressed with this technology, as well as the IMS instrumentation.

ALGAE DIVERSITY AND BIOCHEMISTRY

Algae are aquatic macro- and microorganisms and are found in practically all lighted, moist environments including marine habitats, lakes, streams, and wetlands but can also be found growing on snow (e.g., watermelon snow) and are present in many soils. Algae occur in both planktonic (suspended in the water column) and benthic (bottom-dwelling) forms. Algal IMS research has focused on marine and freshwater species.

Algae are classified into 13 divisions based in part on structural attributes such as cell wall composition, pigment content, and energy storage molecules. The three groups that contain the largest number of identified species are the green algae (Chlorophyta), diatoms (Bacilliariophyta), and cyanobacteria (Cyanophyta). The majority of algal IMS research has been conducted on these three groups but has also included red algae (Rhodophyta) (17–20), euglenoids (Euglenophyta) (21), and dinoflagellates (Dinophyta) (22, 23).

There are approximately 6500–20,000 species of green algae, 5000–12,000 species of diatoms, and 1200–5000 species of cyanobacteria identified (2). Generally, green algae have a cell wall made up of primarily cellulose and pectin and store food mainly as starch. Major photosynthetic pigments are chlorophylls *a* and *b*, and accessory pigments of carotenoids and xanthophylls. Diatom cell walls are predominantly silica with some cellulose. Diatom cellular energy is stored as carbohydrates (e.g., leucosin) and lipids. Major diatom photosynthetic pigments include chlorophylls *a* and *c*, with accessory pigments of carotenoids, xanthophylls, and fucoxanthin. Cyanobacteria (also referred to as blue-green algae) are bacteria rather than algae but are often included in algal ecological studies because of similar size, morphology, and ecosystem function (i.e., primary productivity and nutrient cycling). Cell walls are composed primarily of peptidoglycan, energy is stored mainly as glycogen, and chlorophyll *a* and phycobillins are the major photosynthetic pigments.

Algal IMS research has focused on several macromolecular pools, including proteins (amide I and II), lipids (methyl and methylene groups, esters), carbohydrates (starch, cellulose), nucleic acids and phosphoryl groups, and silicate (in diatoms and cyanobacteria). Table 1 lists the major macromolecular bands and vibrational frequency assignments associated with algae. Green algae, diatoms, and cyanobacteria have distinct chemical composition that can be observed in the infrared absorption spectra (Figure 1). Typically, green algae have a relatively high starch and cellulose content (cell walls and energy storage products) from $\sim$1100 to 900 cm^{-1} (24, 25), diatoms have a distinctive silicate

Table 1. Range of major FT-IR band assignments reported for algal analysis

Wavenumber range	Assignments	Functional groups	Comments
3750	Si_8O—H	Silica	(29)
3400–3300	v O—H/v N—H	Water, protein	(23, 29)
2970–2960	$v_{as}CH_3$	Lipids	Methyl groups (29, 43)
2930–2920	$v_{as}CH_2$	Lipids	Methylene groups (23, 29, 43)
2875–2850	v CH_2, CH_3	Lipids	Methyl and methylene groups in fatty acids (29, 43)
1745–1734	v C=O of esters	Membrane lipids, fatty acids	(23, 26, 27, 29, 43)
1720–1700	v C=O of esters	Carboxylic group of esters	(27, 29)
1655–1638	v C=O	Protein (Amide I)	Protein. May also contain C=C stretches of olefinic and aromatic compounds (23, 26, 27, 29, 40, 43)
1630	v O-H	Water	(29)
1699–1590	v_{as} COO—	Carboxylic group	(40)
1545–1540	δ N—H, v C—N	Protein (Amide II)	Protein (23, 26, 27, 29, 40, 43)
1456–1450	δ_{as} CH_2, δ_{as} CH_3	Lipid, protein	Methylene peaks of lipid (23, 26, 27, 29, 40, 43)
1460–1392	v C—O	Carboxylic group	(27, 29, 40)
1398–1370	δ CH_3, δ CH_2/δ C-O	Proteins, carboxylic groups	(23, 26, 27, 29, 40, 43)
1320	v C—H, δ N—H	Proteins	(40, 43)
1255–1250	v_{as} S=O		(17, 40)
1244–1230	v_{as} P=O	Nucleic acids, phosphoryl group	DNA/RNA backbones, phosphoralated proteins and polyphosphate storage products (23, 26, 29, 43)

1215	v S=O		(40)
1200–900	v C—O—C/v_{as} P=O	Polysaccharides/nucleic acid	Mainly polysaccharide rings / DNA/RNA (26, 29, 43)
1165, 1152, 1110, 1081, 1050, 1030	v C—O	Cellulose	(23, 29)
1150–1000	v C—O/v Si—O	Polysaccharides / siloxane	Carbohydrate peaks/siloxane shoulder at 1200 cm[1] (29)
1090–1030	v P=O	Nucleic acids	(27, 29)
1090–1020	v Si—O		(26, 27)
1030	v O=S=O	Sulfate	(20)
980–940	P—O—P	Polyphosphate	(27)
950	v Si—H/v Si—OH	Silane / silanol	(29)
840	C_4—O—S	Sulfate	(19)
800	v Si—O	Siloxane / SiO_4 ring	(29)

v = symmetric stretch, v_{as} = asymmetric stretech, δ = symmetric deformation (bend), δ_{as} = asymmetric deformation (bend) References for band assignments are in parentheses.
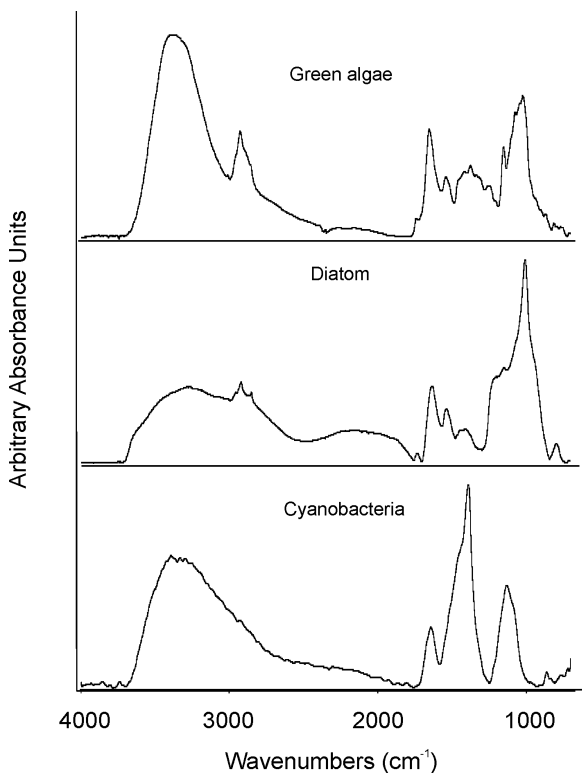
Figure 1. Typical spectra for three dominant algal groups, green algae, diatoms, and cyanobacteria. Distinct differences include abundant carbohydrate (1200–900 cm^{-1}) in green algae, and a prominent silica band ($\sim$1060 cm^{-1}) in diatoms. Cyanobacteria spectra are similar to green algae but often have more distinct protein bands and lack cellulose, particularly in cell walls.

absorption at $\sim$1100–1060 cm^{-1} and $\sim$800 cm^{-1} due to a silica frustule (cell wall) (26, 27), and cyanobacteria spectra are dominated by protein and lipid with less abundant carbohydrates relative to green algae (28, 29). However, the proportions of these macromolecular pools can vary substantially among species within these groups and with nutrient availability (26, 30, 31).

IMS APPROACHES AND EXPERIMENTAL CONSIDERATIONS

Biological and ecological algal IMS approaches differ in both their questions and experimental execution. Whereas a biological approach is concerned with the chemical and physiological composition of algae, an ecological approach focuses on the interactions between an individual (or population) and

its environment, and questions tend to center on population or community implications, rather than individual organisms. Biological and ecological approaches are not mutually exclusive because knowledge of basic cell structure is vital to understanding cellular physiological responses to their environment. There has been a progression in algal IMS research from a strictly biological approach toward more ecological-based questions and specifically toward algal responses to varying nutrient availability. Nevertheless, the continued advancement of imaging resolution and speed of data acquisition has increased the ability to measure whole cell and subcellular content, and will further advance our knowledge of basic cell structure and physiology.

Care must be taken to design experiments that can adequately address the natural variability in cellular content (21, 32), which often requires numerous replicate measurements. There is little information on the physiological diversity of individual species within a natural assemblage, because our knowledge in this area is based mostly on laboratory cultures (but see Murdock et al. (25) and Sigee et al. (33)). Algae can be very plastic concerning nutrient stiochiometry and macromolecular pool content, shifting the relative proportion of protein, lipids, carbohydrates, etc., with nutrient availability. Additionally, the current stage of the cell cycle can greatly impact its macromolecular content (34). Unfortunately, the range of variability of most species is not known and is often a question of concern in IMS algal studies (23, 25, 32, 35).

Algal habitat must be taken into consideration when designing experiments and analytical procedures because planktonic and benthic algae develop in very different conditions. Phytoplankton can theoretically acquire nutrients from all directions, there is relatively more distance between suspended individuals, which can reduce competition and cells can move relatively quickly into different levels of nutrient and light availability. Conversely, benthic algae grow in a complex three-dimensional matrix of many species with varying shapes, sizes and competitive ability. At the microbial scale, molecular diffusion rates often limit nutrient movement from the overlying water in all but the surface of the biofilm, and overlaying cells can significantly shade cells below them (36). Thus, the spatial location within the biofilm can greatly influence nutrient and light availability, which is vital to photosynthetic organism metabolism and reproduction.

Microalgae cell size can vary from approximately 1 to 300 μm, and cells can occur singularly, as colonies of various shapes and cell numbers and branched and unbranched filaments. Therefore, the method chosen to analyze cells—e.g., synchrotron vs. thermal IMS, individual spectra vs. images, aperture size, and number of measurements needed—depends greatly on the actual research question. For example, many algal investigations can be undertaken using a conventional (thermal) infrared source, which may be preferred in studies where many measurements need to be done quickly after collection and inexpensively. However, the enhanced spatial resolution achievable with synchrotron confocal IMS may be necessary to analyze the smallest algal species or provide increased subcellular resolution.

Analysis efficiency is imperative in ecologically based studies because of the large number of measurement that may be needed to offset the natural variability in cell nutrient composition. Typically, applying an aperture size that most closely reflects the target cell size should be used to get the best estimate of whole cell content. Thus, point measurements can be very effective. Alternatively, imaging whole cells can be an important tool for understanding subcellular changes and close spatial relationships among cells, such as cells in the same colony or different species that grow attached to one another.

APPLICATIONS

Algal research with IMS is relatively new but shows great potential in understanding both algal biology and ecology. A summary of algal IMS research to date is presented in Tables 2–4, highlighting the instrumentation used (Table 2), the algal groups investigated with instrument collection settings (Table 3), and major research goals (Table 4). In many of these studies other techniques were used in conjunction with IMS to address research hypotheses.

Sample Preparation

Most algal cells are suitable for IMS analysis with little preparation. Microalgae typically have adequate thickness and infrared transparency without sectioning or other processing and contain enough cellular material to achieve a good IR signal. However, larger marine macroalgae typically require sectioning to a thickness of 10–20 μm (17–19). Sample preparation is similar for both planktonic and benthic microalgae and is straightforward, simple, and relatively fast. Algae grown in culture are collected, concentrated with a centrifuge, rinsed with deionized water to remove culture medium, and then placed on an infrared transparent disc or reflective slide. Benthic algal are scraped/brushed from the substratum, rinsed, and placed on an appropriate infrared disc or slide. Filamentous algae are floated on a few drops of deionized water and manipulated with tweezers so that filament branches or adjacent filaments spread out (25). Algae are then dried in a laminar flow environment and, if necessary, stored in a desiccator until analysis. Alternatively, algae can be grown directly on an infrared reflective surface and then dried and examined without disturbing natural spatial locations (37). However, care must be taken to stop colonization before a multilayer biofilm develops, limiting analysis to early successional stages of development.

Cellular Composition

Initial investigations with IMS focused on the molecular composition of larger marine algae (i.e., seaweeds), and specifically cell wall content. Sekkal and

Table 2. Peer reviewed algal FT-IR microspectroscopy research (1993–2009). Microspectroscopy equipment used in each study.

Reference	FT-IR Spectrometer	Microscope	Infrared Source
30 Beardall et al., 2001	Bruker IFS-55 Equinox	Bruker IRscope II	Thermal
28 Benning et al. 2004a	Nicolet 730	Nicolet Nic-Plan	Synchrotron, Darsbury Laboratory, Warrington, UK
29 Benning et al. 2004b	Nicolet 730	Nicolet Nic-Plan	Synchrotron, Darsbury Laboratory, Warrington, UK
40 Chiovitti et al. 2008	Varian FTS 7000	Varian UMA600	Thermal
35 Dean and Sigee 2006	Nicolet 730	Nicolet Nic-Plan	Synchrotron, Darsbury Laboratory, Warrington, UK
23 Dean et al. 2007	Nicolet 760 FTIR	Spectra-Tech Nic-Plan IR	Synchrotron, Lawrence Berkley National Laboratory, Berkley, CA, USA
24 Dean et al. 2008a	Nicolet Nexus FTIR	Nicolet Continuμm IR	Synchrotron, Darsbury Laboratory, Warrington, UK
45 Dean et al. 2008b	Nicolet 760 FTIR	Nic-Plan IR	Thermal
39 Dunn et al. 2007	Nicolet 760 FTIR	Nicolet Continuμm IR	Thermal
20 Fournet et al. 1997	Bruker IFS 88	Brucker A590	Thermal
26 Giordano et al. 2001	Bruker IFS-55 Equinox	Brucker A590	Thermal
43 Heraud et al. 2005	Nicolet Nexus FTIR	Nicolet Continuμm IR	Synchrotron, Darsbury Laboratory, Warrington, UK
32 Heraud et al. 2008	Perkin elmer Spotlight 2000	Perkin Elmer	Thermal
21 Hirschmugl et al. 2006	Thermo Nicolet 560	Thermo Nicolet Nic-Plan	Synchrotron, Synchrotron Radiation Center, Stoughton, Wl, USA
42 Kansiz et al. 1999	Brucker IFS-55 Equinox	Bruker IRscope II	Thermal
22 Kokinos et al. 1998	Nicolet/Spectra-Tech Irus/SIRM	Nicolet	Thermal
34 Liang et al. 2006	Varian FTS 7000	Varian, model 600 UMA	Thermal
41 Lin and Ritz 1993	Digilab FTS-60	Digilab UMA-300	Thermal
25 Murdock et al. 2008	Perkin Elmer	Perkin Elmer Spotlight 300	Thermal
37 Murdock and Wetzel	Nicolet Magna 850	Nicolet Continuμm IR	Synchrotron, National Synchrotron Light Source, Brookhaven, NY, USA
47 Patel et al. 2008	Bruker Equinox 55	Bruker Hyperion 3000	Thermal
17 Sekkal et al. 1993a	Bruker IFS 88	Bruker	Thermal
18 Sekkal et al. 1993b	Bruker IFS 88	Bruker	Thermal
19 Sekkal et al. 1993c	Bruker IFS 88	Bruker	Thermal
33 Sigee et al. 2002	Nicolet 730	Nicolet Nic-Plan	Synchrotron, Darsbury Laboratory, Warrington, UK
44 Sigee et al. 2007	Nicolet Nexus FTIR	Nicolet Continuμm IR	Synchrotron, Darsbury Laboratory, Warrington, UK
31 Stehfest et al. 2005	Bruker Vector 22	Bruker A590	Thermal
38 Toole et al. 2004	Bio-Rad FTS 175C	Bio-Rad UMA-500	Thermal
27 Vardy and Uwins 2002	Perkin Elmer System 2000	Perkin Elmer	Thermal
46 Yee et al. 2004	Nicolet 760 FTIR	Spectra-Tech Nic-Plan IR	Synchrotron, Lawrence Berkley National Laboratory, Berkley, CA, USA

Table 3. Peer reviewed algal FT-IR microspectroscopy research (1993–2009). Algae characteristics and data acquisition settings in each study.

Reference	Algae	Algal Size Group	Algal Source	Spot Size (μm)	Spectral Resolution	Scans Coadded	Point/Image
30	Green, cyanobacteria, diatom	Micro	Culture, lake	50×50	8	512	Point
28	Cyanobacteria	Micro	Culture	20×10	8	256	Point
29	Cyanobacteria	Micro	Culture	20×10	8	256	Point
40	Diatom	Micro	Culture	5.5×5.5	6	128	Image
35	Cyanobacteria	Micro	Lake	10×10	4	128	Point
23	Cyanobacterium, dinoflagelate	Micro	Lake	10×10	4	64	Point
24	Green	Micro	Culture	50×50	4	64	Point
45	Cyanobacterium	Micro	Culture	10×10	4	64	Point
39	Coraline alga	Macro	Culture	150×150	8	128	Point
20	Red	Macro	Bay	29×29	4	200	Point
26	Diatom	Micro	Culture	30×80	8	10	Point
43	Green	Micro	Culture	20×20, 10 μm step	8	32	Line map, image
32	Green	Micro	Culture	35×35	8	32	Point
21	Euglena	Micro	Culture	5×5, 5 μm steps	8	512	Point/image
42	Cyanobacteria, green	Micro	Culture	80×80	8	10	Point
22	Dinoflagellate	Micro	Culture	20 20, 100×100	4	128, 256, 512	Point
34	Diatoms	Micro	Culture	250×250	6	32	Point

41	Green, unknown filament	Micro	Fossil	—	8	—	Point
25	Green	Macro	Stream	6×6, 25×25	4	64	Point, image
37	Diatoms	Micro	Stream	10×5, 15×5	6	64	Point, line map
47	Green	Micro	Culture	267×267	8	1	Image
17	Red	Macro	Bay	10×10	4	200	Point
18	Red	Macro	Bay	10×10	2	200	Point
19	Red	Macro	Bay	10×10	4	200	Point
33	Green	Micro	Lake	25×25	4	128	Point
44	Green	Micro	Culture	10×10	4	64	Point
31	Cyanobacteria, diatoms	Micro	Culture	85×85, 374×374	4	200	Point
38	Green	Macro	Culture	100×100	8	64	Point
27	Diatoms	Micro	Culture	25×25	8	50	Point
46	Cyanobacterium	Micro	Culture	10×10	8	512	Point

Table 4. Peer reviewed algal FT-IR microspectroscopy research (1993–2009). Research goals and spectral analysis in each study.

Reference	Macromolucules of Interest	Focus of study/Comments	Spectral Statistics
30	Protein, carbohydrate, phosphodiester, lipid, silica	Comparison of methods to measure algal P limitation	Peak ratios
28	Silica, protein, carbohydrate, nucleic acid, lipid	Assess changes in pools in cells and cell sheaths with progressive silicification	Difference spectra
29	Silica, carbohydrate	Assess changes in carbohydrate and silica structure of cell walls and sheats during silicification	None
40	Silica (1110–1050 cm^{-1}), sulfate (1240–1200 cm^{-1})	Characterize the composition of a diatom adhesive pad	Seond derivative images
35	Protein, carbohydrates, phosphodiesters, lipids	Characterize two algal populations from mixed, natural phytoplankton samples	Pearson correlation analysis, PCA of individual band intensities, and whole spectra
23	Protein, carbohydrates, phosphodiesters, lipids	Characterize two algal populations from mixed, natural phytoplankton samples	PCA, hieracrchial cluster analysis, CV, Spearman correlation analysis
24	Protein, carbohydrates, phosphodiesters, lipids	Change in macromolecules with P limitation over time	Peak ratios
45	Protein, carbohydrates, phosphodiesters, lipids	Change in macromolecules with P limitation over time	Peak ratios, PCA, hierarchial cluster analysis
39	Carbohydrates (mannan, cellulose)	Characterize cell walls of algae and gametes	Difference spectra
20	Carbohydrate (carregeenan), sulfate	Characterize diftent cell layers in cell wall	Peak ratios
26	Protein, carbohydrates, phosphodiesters, lipids, silicon	Change in carbon allocation with two N sources, and under N limitation	Peak ratios
43	Protein, carbohydrates, phosphodiesters, lipids	Change in lipid and protein content over time in N and P limited conditions, used live cells	Peak ratios
32	Protein, carbohydrates, phosphodiesters, lipids	variability in micrcolony populations with P limitation	PCA, SIMCA, PLS-DA
21	Protein, carbohydrate	Classification of macromolecules in nutrient replete and nutrient limitation	Agglomerative hierarchical cluster analysis

42	Protein, carbohydrates, phosphodiesters, lipids	Discrimination of algal strains	PCA, hieracrchial cluster analysis
22	Lipids, carbohydrates	Characterize cell wall of algal resting cyst	None
34	Protein, carbohydrates, lipids	Change in macromolecules with culture age	Peak ratios
41	Aliphatic C-H (3000-2800 cm^{-1})	Characterize fossil algae remains	Spectral deconvolution and peak area calculation
25	Protein, carbohydrates, phosphodiesters, lipids	Subcellular, ^{15}N isotope uptake	PCA, Hieracrchial cluster analysis, peak area ratios
37	Protein, carbohydrates, phosphodiesters, lipids	Characterize nitrogen variability in a population in a natural biofilm	Peak ratios, PCA
47	Protien, lipids	Change in lipid and protein distribution with pharmaceutical exposure	PLS regression
17	Carbohydrates (agar, carrageenan), sulfate	Characterize cell wall in situ	None
18	Carbohydrates (agar, carrageenan), sulfate, proteins	Characterize spatial variability in cell wall macromolecules	None
19	Carbohydrates (carrageenan), sulfate	Characterize polysaccharides in different species of red algae with varying sulfate concentrations	None
33	Protein, carbohydrates, phosphodiesters, lipids	Characterize a green algal population from mixed, natural phytoplankton samples	Peak ratios, Pearson and Spearman correlation analysis
44	Protein, carbohydrates, phosphodiesters, lipids	Change in macromolecules with P limitation over time	Peak ratios
31	Protein, carbohydrates, phosphodiesters, lipids, silicate	Change in macromolecules with N and P limitation over time	Peak ratios
38	Carbohydrates (cellulose, pectins)	Cell wall chemical composition, stretch sample	Difference spectra
27	Silicate, protein, carbohydrates, phosphodiesters, lipids	Differentiate two species of diatoms	Discriminant analysis using Mahalanobis distance and PCA
46	Protein, carbohydrates, phosphodiesters, lipids	Characterize metal-algal sorption reactions	None

colleagues produced a series of papers on the polysaccharide content in the marine red macroalgae *Gracilaria verrucosa* and *Gelidium latifolium*. Sekkal et al. (17) examined extracted agar, commercially available agar, and agar in intact algal sections. Agar had strong absorption bands between 1100 and 1000 cm^{-1} (C—C, C—O stretching and C—O—H bending) and several weaker absorption peaks from 988 to 716 cm^{-1}. Additionally, sulfate content (which affects agar gelling ability) was observed at 1250 cm^{-1}. This band was attributed to the substitution of sulfate esters (O=S=O asymmetric stretching) on the pyronose rings on the polygalactanes. In later studies of microalgae and freshwater macroalgae, the 1250 cm^{-1} band has been typically assigned to the asymmetric stretching vibration of phosphoryl groups (P=O asymmetric stretch) in nucleic acids and phosphorolated compounds (23, 26, 28). Sekkal et al. (18) found that cell walls also contained abundant protein, because strong amide I and amide II bands occurred at ∼1645 and 1530 cm^{-1}, respectively.

Thallus (i.e., stem) sections from four spatial disparate areas of *G. verrucosa* showed that there was little difference in macromolecular composition among these locations and that agar abundance varied within the thallus with greater concentrations toward the outside walls. Sekkal et al. (19) studied three additional marine macroalgae species and found similar macromolecular distribution among species. Distinct spatial distributions of macromolecules within the thallus were substantiated by Fournet et al. (20), who found differences in the carrageenan content and sulfate substitution in different cell layers of the thallus (i.e., cortex, subcortex, and medulla) of the red marine macroalga *Solieria chordalis*. Peak height ratios at 805 cm^{-1} (C—O—S), 930 cm^{-1} (C—O—C), 1050 cm^{-1} (C—C), and 1250 cm^{-1} were used to measure changes in the polysaccharide content and sulfate substitution among cell layers and in algae with and without carrageenan extraction.

The chemical composition of a green macro-algal (*Chara coralline*) cell wall was studied by Toole et al. (38). Unlike red algae, spectra indicated that cellulose (bands at 1162, 1060, 1030 cm^{-1}) and pectin (bands at 1610, 1424, 960 cm^{-1}) were the major cell wall components. Cyclohexane-trans-1,2-diamine-N,N,N′, N′ -tetraacetate (CDTA) extraction of pectin showed the presence of polygalacturonic acid (PGA) with bands at 1608, 1425, 1095, 1009 cm^{-1}.

The marine macroalga *Acetabularia acetabulum* is a unicellular green alga with distinct morphological features such as an upright 3- to 4-cm-tall stalk, a basal rhizoid for attachment, and a cap that houses gametes. Infrared microspectroscopy detected distinct compositional differences between stalk and gamete cell walls. Gametes had peaks at 1161, 1107, 1060, and 1038 cm^{-1} (characteristic of cellulose), whereas stalk wall spectra exhibited additional peaks at 1146 and 1078 cm^{-1}, suggesting both cellulose and mannan were present (39).

Kokinos et al. (22) examined the cell wall composition of the resting cyst of the marine dinoflagellate *Lingulodinium polyedru*, which can protect the cell

from extreme temperatures and desiccation. Spectra collected during a series of solvent extraction, saponification, and acid hydrolysis showed abundant long chain fatty acids (e.g., CH_2/CH_3, carboxylic acids (C—O), and hydroxyl groups (O—H)). Spectra from this algal cyst closely resembled that of previously published spectra of spore cell walls of *Lycopodium* (a club moss).

Synchrotron IMS was used to assess the silicification process of cyanobacteria filaments (*Calothrix* sp.) and overlying sheath material (28). Spectra of whole cells and purified sheaths showed a distinct progression of silica formation (i.e., increase in the bands associated with silica) on whole cells and mechanically altered sheaths. A broad peak from 1190 to 1069 cm^{-1} (Si—O/C—O stretch of siloxane and polysaccharides) and a more distinct Si—O stretch at 800 cm^{-1} were used to detect silicification. Benning et al. (29) further found a two-stage process of silica mineralization on cell surfaces using changes in the integrated curve areas (1150–950 cm^{-1} and 800 cm^{-1}) to derive changes in silica content of cells and sheaths. The 1150–950 cm^{-1} band that includes both siloxane and polysaccharides increased proportionality with increasing silica concentration in the water. The initial band increase was due to polysaccharide accumulation in a thickening sheath. However, a shift to predominantly siloxane attachment to the outside of the sheath occurred. This second step was detected by a delayed increase in the 800 cm^{-1} band during the process.

Chiovitti et al. (40) analyzed the adhesive pads of the benthic diatom *Toxarium undulatum*. The extracellular pads contained proteins dominated by β-sheet structure, rather than the α-helix structure that dominates internal cell material such as chlorophyll, and pads were mostly composed of silicate and sulfate compounds. Silicate and sulfate concentrations within the pads were localized with second derivative images of the integrated area under the curves at 1110–1050 cm^{-1} and 1240–1200 cm^{-1} for silicate and sulfate, respectively.

Nutrient variability among cells along filaments and within single cells of the filamentous green macroalga *Cladophora glomerata* ($\sim 25 \times 250$ μm cell size) were studied by Murdock et al. (25). Among-cell variability was high but consistent among macromolecular pools with coefficients of variation ranging from 32 to 53% for proteins (1655 and 1545 cm^{-1}), carbohydrates (1025 cm^{-1}), lipids (2927 cm^{-1}), and phosphoryl groups (1240 cm^{-1}). Subcellular protein and lipid content were highly spatially correlated and concentrated at cell tips and nodes, which are regions of greatest cell growth.

Fossil Algae

Infrared microspectroscopy has been used to study fossil remains of ancient algae in organic rich shales. Lin and Ritz (41) found intense aliphatic C—H hydrocarbons (stretching 3000–2800 cm^{-1}, and deformational 1500–1300 cm^{-1}) in unicellular (*Tasmanites*), colonial (*Botryococcus braunii*), and filamentous (unknown) algae, but very little aromatic (C=C—H) hydrocarbons.

Aliphatic to aromatic ratios were calculated with *B. braunii* having the highest ratio. Increased aliphatic content increases the likelihood of petroleum presence within the rock formation.

Species Differentiation and Classification

Algal species within major groups can be differentiated by their infrared absorption spectra. Kanzis et al. (42) differentiated five species of cyanobacteria (including two strains of *Microcystis aeruginosa*) and a green alga (*Chlorella emersonii*) using first derivative spectra in the 1800–950 cm^{-1} region. Two classification methods based on principal components analysis (PCA) were used to classify algal species with a highest correct classification rate of 99–100%. Infrared microspectroscopy can also be used as a tool to differentiate two species with very similar physical characteristics that are difficult to separate with light microscopy. Vardy and Uwins (27) compared spectra of two similar diatom species, *Nitzschia closterium* and *N. longissima*. Silica content ($\sim$1075 cm^{-1}) was found to be the major differentiating feature using discriminate analysis based on Mahalanobis distances and PCA, followed by canonical discriminate analysis.

Sigee and Dean published a series of papers assessing population variability, and classified microalgae from natural lake assemblages. Band areas and area ratios of major molecular pools in algae including lipids (2924 cm^{-1}), protein (1650 and 1542 cm^{-1}), nucleic acids (1077 cm^{-1}), cellulose (1739 cm^{-1}), and starch (1151 and 1077 cm^{-1}) were measured. Correlation and factor analyses showed that variations in lipids and protein were highly correlated among individuals of the green alga *Pediastrum duplex*, whereas changes in carbohydrates were unrelated to other bands (33). Correlation and PCA were used to compare two species of cyanobacteria (*Aphanizomenon flos-aquae* and *Anabaena flos-aquae*) from different depths within a lake (35). PCA was performed on the region from 1750 to 900 cm^{-1} and loading plots were used to determine which bands were responsible for sample differentiations. Species differed mostly in protein, nucleic acid, and phosphorus compounds. Within-species nutritional variation due to depth was observed in *Aphanizomenon* (Figure 2) but not *Anabaena*.

A cyanobacterium (*Microcystis aeruginosa*) and a dinoflagellate (*Ceratium hirundinella*) from natural lake populations were differentiated using cluster analysis and three-dimensional principle components factor plots (23). Both methods showed a clear separation of the two species but highlighted high variability in band intensities associated with natural populations. The authors also caution that perceived differences in algal spectra may be influenced by the current environment and growth stage.
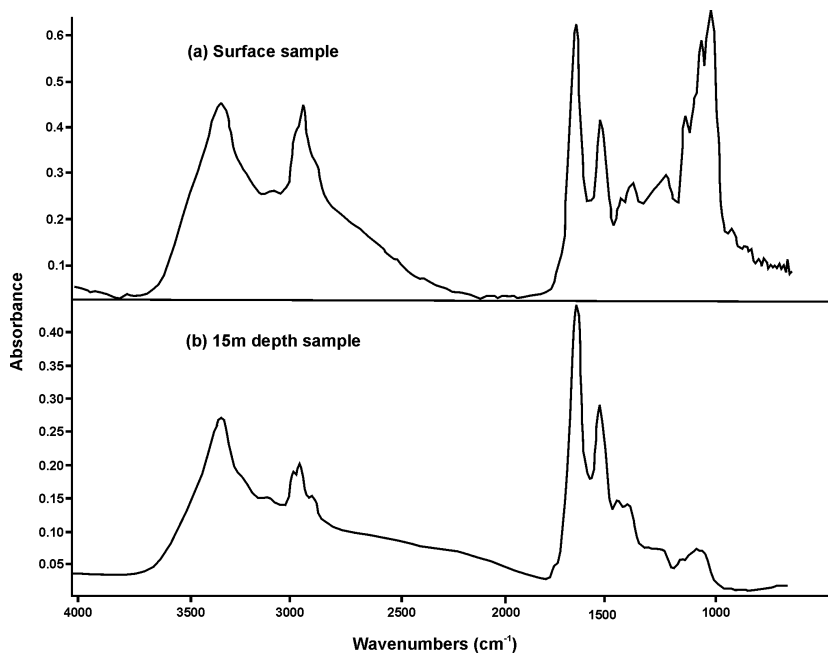
Figure 2. Spectra of lake cyanobacteria (*Aphanizomenon flos-aquae*) from the (a) surface and (b) 15 m depth. FT-IR spectra showed clear macromolecular differences (protein-to-carbohydrate ratio) between surface algae and algae taken from depth. Redrawn from Dean and Sigee (35) with permission from Taylor and Francis.

## Species-Specific Responses to Nutrient Availability

Algal species have evolved to partition out available resources; i.e., some are better competitors under certain environmental conditions than others. Each species should thus have a distinct response to changing conditions. Understanding which species will likely dominate given the current conditions can help predict assemblage characteristics such as biomass, edibility, productivity, and nutrient uptake potential. Species-specific measurements can allow the study of in situ microbial competition and provide new insight into competition among major groups (i.e., green algae and diatoms), closely related species, and species with similar morphologies and life histories.

Several research groups have investigated microalgal responses to varying nutrient availability, using both algal cultures and natural populations. However, groups associated with Monash University, Clayton, Australia, have published the majority of the papers on this topic. In general, N and P limitation causes

an increase in lipid and carbohydrate relative to protein and phosphoryl groups in algae. This pattern was observed in green algae, diatoms, and cyanobacteria.

Giordano et al. (26) studied nitrogen limitation in the planktonic marine diatom, *Chaetoceros muellerii*. Cultures of *C. muellerii* were grown in N replete and depleted conditions (using two ionic sources of nitrogen, NH_4^+ and NO_3^-) to determine how carbon allocation patterns change (i.e., distribution of proteins, carbohydrates, and lipids) with nitrogen availability. Algal amide I and II bands ($\sim$1650 and $\sim$1540 cm^{-1}, respectively) from both the NH_4^+-rich and NO_3^--rich environments were reduced when cells were placed in a nitrogen free media. Amide bands were enhanced when cells were reintroduced to NH_4^+-rich and NO_3^--rich media. As nitrogen became limiting, cellular carbon shifted from proteins and carbohydrates into lipids (the C=O stretch of ester carbonyl group, $\sim$1740 cm^{-1}). This reallocation was greater when NO_3^-, rather than NH_4^+, was the N source. The band from the diatom's silica frustule ($\sim$1075 cm^{-1}) obscured a large portion of the nucleic acid and carbohydrate regions. However, this band was used to normalize spectra from different *C. muellerii* cells because it had a constant intensity regardless of N availability.

Beardall et al. (30) used IMS to assess P limitation in four species of cultured algae, *Phormidium luridum*, *Nitzschia* sp., *Scenedesmus quadricauda*, and *Sphaerocystis schoeteri*. Carbohydrates (C—O stretching vibrations at 1024, 1080, and 1150 cm^{-1}) and lipids (CH$_2$ stretching vibrations at 2924, 2854, and 1737 cm^{-1}) increased under P limiting conditions. When P was reapplied, an increase in the phosphodiester bands at 1244 and 1080 cm^{-1} was observed in conjunction with a decrease in carbohydrates and lipids. Figure 3 shows spectral changes in the green colonial alga *Sphaerocystis schoeteri* during P limitation and 24 h following the resupply of P.
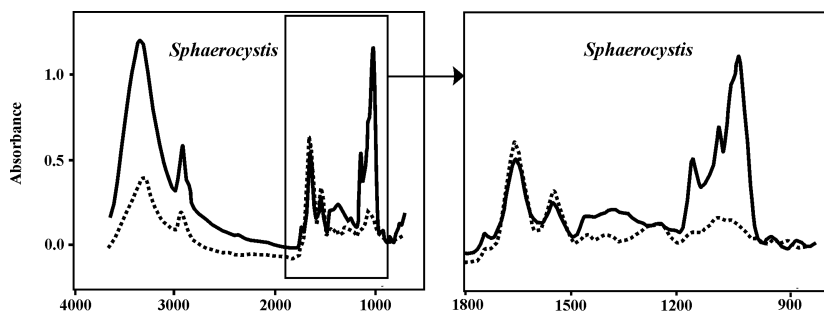
Figure 3. FTIR spectra of the green colonial alga *Sphaerocystis schoeteri* during P limitation (solid line) and 24 h following the resupply of P (dashed line). The right panel is an enlargement of the boxed region in the left panel highlighting the decrease in lipids (C=O ester carbonyl stretch at 1737 cm^{-1}) and a fivefold decrease in carbohydrates (C—O stretching vibrations at 1024, 1080, and 1150 cm^{-1}) after P resupply. Redrawn from Beardall et al. (30) with permission from Springer-Verlag.

Liang et al. (34) studied how macromolecular content of two diatom species (*Phaeodactylum tricomutum* and *Chaetoceros muellerii*) changed with culture age. In both cases, lipid (C−H stretching between 3800 and 2800 cm^{-1} and C=O ester at 1740 cm^{-1}) increased with age, whereas protein (amide I and amide II) decreased in *P. tricomutum*, and carbohydrate (C−O−C bands between 1200 and 1000 cm^{-1}) decreased in *C. muellerii*.

Heraud et al. (32) studied the variability of macromolecules within a culture population of the green alga *Scenedesmus quadricauda* exposed to P replete and P limited conditions. Algal microcolonies in P limited conditions had lower protein proportions and increased carbohydrate (C−O stretching at 1200–1000 cm^{-1}) proportions. There was little difference in phosphodiester bands (∼1240 cm^{-1}) or lipids (1740 cm^{-1}). P starved cells were also more variable in macromolecular content than P replete cells.

Heraud et al. (43) developed a model system for analysis of a single live algal cell under changing nutrient availability. An infrared transparent flow-through chamber was constructed of a 3-mm-thick CaF_2 lower window and a 2-mm-thick ZnSe upper window, creating a 12-μm space. This chamber kept a single living green algae cell, *Micrasterias hardyi*, in place while allowing nutrient amended water to flow past. Algal cells remained viable in this chamber for up to one day and allowed analysis of hydrated cells. Figure 4 illustrates the potential spatial subcellular artifacts that can arise from the analysis of dried cells, as dried cells showed distinctly different protein and lipid distribution within *M. hardyi*.

Linemaps were made across the center of cells through the nuclear region perpendicular to the isthmus. Spectra were collected at periodic intervals after the additional of P and N for 615 and 1380 min, respectively. *M. hardyi* cells depleted of P had increased lipid content but did not return to prestressed condition within 10 h of exposure to P replete conditions. N starvation caused a decrease in protein, but resupply of N did not increase the amide II band during the 23 h cells were monitored. Unlike previous findings, lipid decreased with N starvation.

Additional work on algal response to nutrient availability was undertaken by Stehfest et al. (31). Changes in the IR spectra of three planktonic cyanobacteria (*Microcystis aeruginosa*, *Chrococcus minitus*, *Nostoc* sp.) and two diatoms (*Cyclotella meneghiniana*, *Phaeodactylum tricomutum*) were studied with laboratory cultures subjected to N or P nutrient stress (a 10% reduction in ambient nutrient concentrations) over 35 days. Ratios of lipid/amide II, carbohydrate/amide II, and lipid/phosphor bands increased with reduced nutrient availability. Spectra form the cultured *Microcystis* were compared to a population of *Microcystis* collected from a eutrophic lake. Lake spectra closely matched the spectra of N depleted cells and the authors suggest N limitation is present in the natural population.

Stehfest et al. (31) also examined macromolecule loss in *C. meneghiniana* exposed to extended periods without light. The diatom showed a well-defined
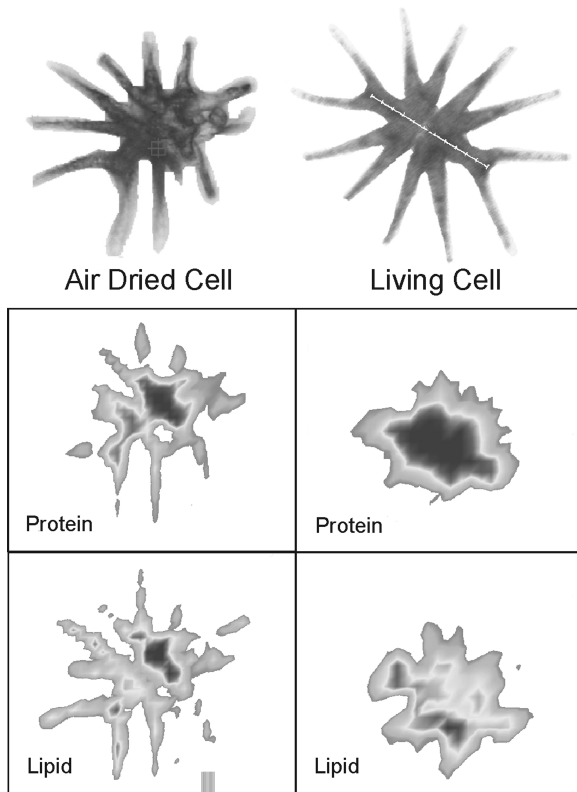
Figure 4. Infrared microspectroscopy images of air-dried and live *Micrasterias hardyi*. Images show differences in lipid (ester carbonyl 1750–1720 cm^{-1}) and protein (amide II, 1565–1515 cm^{-1}) distribution between live and dehydrated cells. Darker areas denote higher concentration. Reproduced from Heraud et al. (43) with permission from Elsevier.

sequence of cell energy storage breakdown. Lipids decreased first, followed by carbohydrates, and then a slow loss of proteins. The authors suggest that short-term exposure to altered nutrient availability is initially visible in changes in pigmentation and photosynthetic ability and that these changes over a longer time period are what lead to assemblage composition changes.

Synchrotron IMS was used to identify subcellular variability in algae. Single cells of *Euglena gracilis* were collected from nutrient replete or nutrient deplete media (21). Whole cells were imaged at a resolution of 5 μm $\times$ 5 μm using vector-normalized, first-derivative spectra. Agglomerative hierarchical clustering analysis of whole spectra (4000–800 cm^{-1}) was used to relate spectral (biochemical) differences to spatial location within a cell. Nutrient depleted cells were more homogenous in macromolecular content and contained a

10-fold lower protein-to-carbohydrate ratio and a fivefold lower lipid-to-protein ratio.

In addition to their work in natural lake assemblages, the group from the University of Manchester reported a series of experiments on the temporal changes in macromolecules with varying P availability. P limited *Scenesdesmus subspiccatus* (a green alga) had higher lipid/protein and carbohydrate/protein ratios than cells grown in intermediate or high P availability conditions during the log phase of growth (44). During the stationary phase, the carbohydrate/amide I ratio increased in all three P treatments; however, the lipid/protein ratio remained relatively unchanged in the intermediate and high P conditions. When P was resupplied, carbon allocation was reversed, leading to lower lipid/protein and carbohydrate/protein ratios. The green alga *Chlamydomonas reinhardtii* had a similar temporal response as *S. subspiccatus* to P limitation and P resupply (45). The macromolecular ratio of the cyanobacterium *Anabaena flos-aquae* did not differ temporally (i.e., on days 8, 12, and 16) (24). P limited *A. flos-aquae* had increased carbohydrate/amide I ratios under P limitation, but lipids were not a major component of these cells because no distinct band ∼1736 cm^{-1} occurred.

Murdock and Wetzel (37) studied macromolecular variability in intact algal biofilms grown directly on infrared reflective slides. Slides were collected after 7 days, producing a single layer of diatom cells. Synchrotron IMS was used to measure the macromolecular changes in the dominant diatom *Achnanthes affinis* ($5 \times 10 \ \mu$m) after exposure to a decrease in N availability (450 to 220 μg N L^{-1}). Lipid/protein ratios increased rapidly within 3 h, even though the lower N concentrations have been shown to support excessive algal growth in the study streams.

Nutrient Uptake

Competitive dominance for nutrients among species and in different locations within the biofilm can be inferred by looking at shifts in macromolecular composition over the timescale of days or weeks. However, short-term uptake ability in natural assemblages can be examined by tracking the gradual incorporation of heavy isotopes of nutrients, such as ^{15}Nitrogen (^{15}N). Because absorption frequency is dependent upon the weight of the vibrating atoms, the incorporation of ^{15}N can be observed by a shift in the amide II band to a lower wavenumber.

^{15}N uptake was tracked into the filamentous green alga *Cladophora glomerata* (25) by measuring the downward shift (1545 to 1535 cm^{-1}) in the amide II (N—H deformation, C—N stretching) band with increasing uptake (Figure 5). The shift was due to a decrease in the 1545 cm^{-1} and increase in the 1535 cm^{-1} peak. ^{15}N incorporation was quantified by using spectral deconvolution
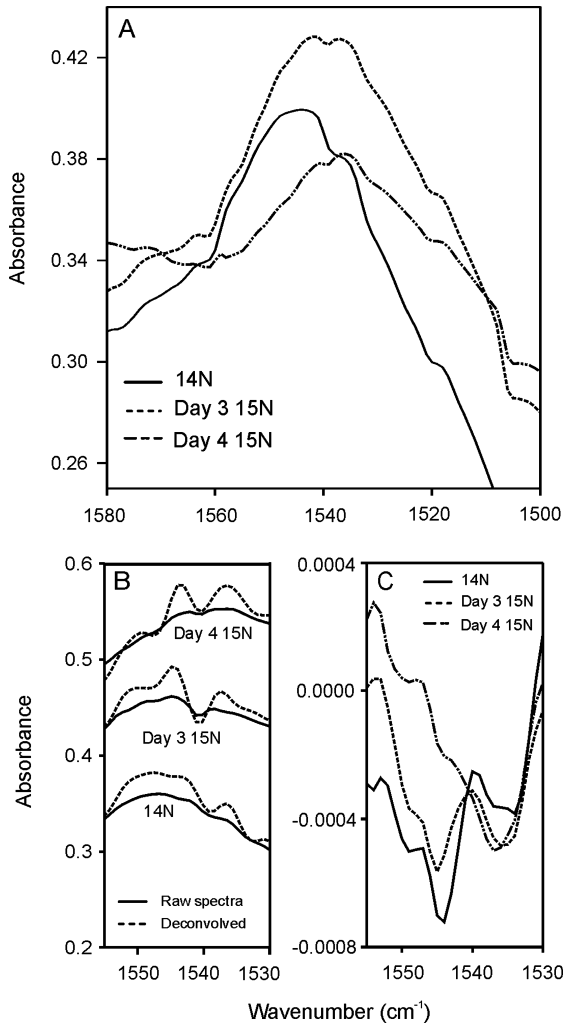
Figure 5. Nitrogen uptake measurements in the green filamentous macroalga *Cladophora glomerata*. (A) A shift in the amide II band occured with increasing [15]Nitrogen uptake after 3 and 4 days. (B) Fourier self-deconvolution of (A), and (C) second derivative spectra of (A) emphasize starting and ending peak positions. The gradual shift is due to a reduction in the 1545 cm^{-1} peak and increase in the 1535 cm^{-1} peak due to replacement of ^{14}N with ^{15}N in the amide functional group in proteins. Reproduced from Murdock et al. (25) with permission from Elsevier.

of the amide II peak and taking the ratio of the integrated area of the 1545 and 1535 cm^{-1} peaks. This method found that ^{15}N uptake from the water increased exponentially in *C. glomerata* filaments approximately 3 mm from their attachment point on a rock.

Metals

pH-dependent metal-algal sorption reactions were studied by Yee et al. (46) using the cyanobacteria *Calothrix* sp. Infrared microspectroscopy was used to characterize macromolecular composition of whole filaments and filament sheaths exposed to a series of pH from 3.6 to 9.3. As pH increased from 4.3 to 6.5, there was a shift in the COO^- symmetrical vibration in the whole filament from 1385 to 1400 cm^{-1}, indicating a progressive formation of deprotonated surfaces. This shift was not observed in isolated sheaths, suggesting increased sites for metal sorption with whole cells over cell sheaths alone.

Pharmaceuticals

Algal physiological reactions to active pharmaceutical ingredients (API) were studied by creating images of whole cells of the green alga *Micrasterias hardyi* exposed to propranolol, metoprolol, and mefenamic acid (47). Images revealed that the central part of the cell is dominated by the amide I (1625 cm^{-1}) band of protein and the outer processes contain more lipid than protein (2946 cm^{-1}/1625 cm^{-1}). Cellular images after API exposure show the protein content decreased within the center of the cell for all three APIs, whereas lipid content is only visually reduced by propranolol.

METHOD LIMITATIONS AND FUTURE RESEARCH

Despite the great potential for algal research with IMS, there are several issues that currently limit its applicability, especially for ecologically based studies. The largest problem is that many spectra are generally needed to get a good understanding of population variability, greatly increasing sample processing time. Additionally, subcellular variability can be high, making it crucial to optimize the image plane mask size and orientation to cell size and shape to obtain representative cell macromolecule content. Spatial resolution is also still a concern. Many important species from all major algal divisions are only a few micrometers, and potentially important interactions may be occurring where cells join or touch. Also, information at lower frequencies can be lost when the image plane mask is smaller than the IR wavelength dimension (typically < 5 μm).

Internal cell content movement with dehydration (especially in diatoms) can be an issue when subcellular macromolecular distribution is of interest. Subcellular shifting can be addressed by using live, hydrated cells in specially constructed sample holders (43); however, these sample chambers must currently be built in-house with dimensions unique to different algal thickness. Alternatively, water substitution or rehydration with deuterium (which absorbs IR light in a different range) has the potential to address this problem (Murdock, unpublished data).

The adaption of IMS to algal ecological research is still in its early stages, and little has been done in natural systems. The stoichiometric plasticity of only a limited amount of the tens of thousands of algal species has been investigated. And we have very little information on the extent of cellular change in natural communities or microbial ecological interactions (25, 33, 35). Most of the focus to date has been on the cellular biology of algae because of the more limited number of spectra needed.

Questions can be addressed with IMS that were previously unanswerable because of the inability to measure the physiologic response of single cells or individual species in natural communities, including measuring species-specific responses to environmental changes and understanding competition among microscopic algae from natural communities. Additionally, this methodology can advance the investigation into which environmental conditions trigger algal bloom formations, increased toxin production, or, in the case of biodiesel production, increased cellular lipid production. Insights from these investigations will shine light on larger ecosystem-scale questions such as understanding the driving mechanisms of succession in the microbial world.

In the future, IMS may be applied to further understand linkages between the microbial food web and higher trophic levels. Organism interactions, such as nutrient transfer among trophic levels, algal assimilation efficiency by grazers, and grazer selectivity (i.e., picking out the most nutritious microbial species) are just a few examples. The most pressing needs at this time, however, include answering basic questions of natural cellular nutrient variability, as well as method development to streamline or automate analysis.

ACKNOWLEDGEMENTS

REFERENCES

1. Mulholland, P.J., Steinman, A.D., Marzolf, E.R., Hart, D.R., and Deangelis, D.L. (1994) Effects of periphyton biomass on hydraulic characteristics and nutrient cycling. *Oecologia*, 98: 40–47.

2. Dodds, W.K. (2002) *Freshwater Ecology: Concepts and Environmental Applications*. Academic Press: San Diego.

3. Anderson, D.M., Gilbert, P.M., and Burkholder, J.M. (2002) Harmful algal blooms and eutrophication: Nutrient sources, composition, and consequences. *Estuaries*, 25: 704–726.

4. Smith, V.H. (2003) Eutrophication of freshwater and coastal marine ecosystems—A global problem. *Environ. Sci. Pollut. Res.*, 10: 126–139.

5. Dodds, W.K., Bouska, W.W., Eitzmann, J.L., Pilger, T.J., Pitts, K.L., Riley, A.J., Schlosser, J.T., and Thournbrugh, D.J. (2009) Eutrophication of US freshwaters: Analysis of potential economic damages. *Environ. Sci. Tech.*, 43: 12–19.

6. Umble, A.K. and Ketchum, L.H. (1997) A strategy for coupling wastewater treatment using the sequencing batch reactor with effluent nutrient recovery through aquaculture. *Water Sci. Tech.*, 35: 177–184.

7. Schumacher, G. and Sekoulov, I. (2002) Polishing of secondary effluent by an algal biofilm process. *Water Sci. Tech.*, 46: 83–90.

8. Kadam, K.L. (2002) Environmental implications of power generation via coal-microalgae cofiring. *Energy*, 42: 905–922.

9. De Morais, M.G. and Costa, J.A.V. (2008) Bioprocesses for removal of carbon dioxide and nitrogen oxide by microalgae for the utilization of gas generated during coal burning. *Quim. Nova*, 31: 1038–1042.

10. Wang, B., Li, Y., Wu, N., and Lan, C.Q. (2008) CO_2 bio-mitigation using microalgae. *Appl. Microbiol. Biotech.*, 79: 707–718.

11. Messerschmidt, R.G. and Sting, D.W. (1989) Microscope having dual remote image masking U.S. Patent 4,877,960.

12. Wetzel, D.L. and Fulcher, R.G. (1990) Fourier transform infrared microspectrometry of food ingredients. In *Flavors and Off-Flavors*, Charalambous, G., Ed. Elsevier: Amsterdam, pp. 485–510.

13. Koc, H. and Wetzel, D.L. (2007) Imaging local chemical microstructure of germinated wheat with synchrotron infrared microspectroscopy. *Spectroscopy*, 22: 24–32.

14. Wetzel, D.L. and Levine, S.M. (1999) Imaging molecular chemistry with infrared microscopy. *Science*, 285: 1224–1225.

15. LeVine, S.M. and Wetzel, D.L. (1993) Analysis of brain tissue by FT-IR microspectroscopy. *Appl. Spectrosc. Rev.*, 28: 385–412.

16. Levenson, E., Lerch, P., and Martin, M.C. (2006) Infrared imaging: Synchrotron vs. arrays, resolution vs. speed. *Infrared Phys. Tech.*, 49: 45–52.

17. Sekkal, M., Legrand, P., Huvenne, J.P., and Verdus, M.C. (1993) The use of FTIR microspectrometry as a new tool for the identification in situ of polygalactanes in red seaweeds. *J. Mol. Struct.*, 294: 227–230.

18. Sekkal, M., Declerck, C., Huvenne, J.P., Legrand, P., Sombret, B., and Verdus, M.C. (1993) Direct structural identification of polysaccharides from red algae by FTIR microspectrometry. 2. Identification of the constituents of Gracilaria-Verrucosa. *Mikrochim. Acta*, 112: 11–18.

19. Sekkal, M., Huvenne, J.P., Legrand, P., Sombret, B., Mollet, J.C., Mouradigivernaud, A., and Verdus, M.C. (1993) Direct structural identification of polysaccharides from red algae by FTIR microspectrometry. 1. Localization of agar in Gracilaria-Verrucosa sections. *Mikrochim. Acta*, 112: 1–10.

20. Fournet I., Gall, E.A., Deslandes, E., Huvenne, J.P., Sombret, B., and Floc'h, J.Y. (1997) In situ measurements of cell wall components in the red alga *Solieria chordalis* (Solieriaceae, Rhodophyta) by FTIR microspectrometry. *Bot. Mar.*, 40: 45–48.

21. Hirschmugl, C.J., Bayarri, Z.E., Bunta, M., Holt, J.B., and Giordano, M. (2006) Analysis of the nutritional status of algae by Fourier transform infrared chemical imaging. *Infrared Phys. Tech.*, 49: 57–63.

22. Kokinos, J.P., Eglintonb, T.I., Goñi, M.A., Boonc, J.J., Martoglio, P.A., and Andersona, D.M. (1998) Characterization of a highly resistant biomacromolecular material in the cell wall of a marine dinoflagellate resting cyst. *Org. Geochem.*, 28: 265–288.

23. Dean, A.P., Martin, M.C., and Sigee, D.C. (2007) Resolution of codominant phytoplankton species in a eutrophic lake using synchrotron-based Fourier transform infrared spectroscopy. *Phycologia*, 46: 151–159.

24. Dean, A.P., Nicholson, J.M., and Sigee, D.C. (2008) Impact of phosphorus quota and growth phase on carbon allocation in *Chlamydomonas reinhardtii*: An FTIR microspectroscopy study. *Eur. J. Phycol.*, 43: 345–354.

25. Murdock, J.N., Dodds, W.K., and Wetzel, D.L. (2008) Subcellular localized chemical imaging of benthic algal nutritional content via HgCdTe array FT-IR. *Vib. Spectros.*, 48: 179–188.

26. Giordano, M., Kansiz, M., Heraud, P., Beardall, J., Wood, B., and McNaughton, D. (2001) Fourier transform infrared spectroscopy as a novel tool to investigate changes in intracellular macromolecular pools in the marine microalga *Chaetoceros muellerii* (Bacillariophyceae). *J. Phycol.*, 37: 271–279.

27. Vardy, S. and Uwins, P. (2002) Fourier transform infrared microspectroscopy as a tool to differentiate *Nitzschia closterium* and *Nitzschia longissima*. *Appl. Spectros.*, 56: 1545–1548.

28. Benning, L.G., Phoenix, V.R., Yee, N., and Tobin, M.J. (2004) Molecular characterization of cyanobacterial silicification using synchrotron infrared microspectroscopy. *Geochim. Cosmochim. Acta*, 68: 729–741.

29. Benning L.G., Phoenix, V.R., Yee, N., and Konhauser, K.O. (2004) The dynamics of cyanobacterial silicification: An infrared micro-spectroscopic investigation. *Geochim. Cosmochim. Acta*, 68: 743–757.

30. Beardall, J., Berman, T., Heraud, P., Kadiri, M.O., Light, B.R., Patterson, G., Roberts, S., Sulzberger, B., Sahan, E., Uehlinger, U., and Wood, B. (2001) A comparison of methods for detection of phosphate limitation in microalgae. *Aquat. Sci.*, 63: 107–121.

31. Stehfest, K., Toepel, J., and Wilhelm, C. (2005) The application of micro-FTIR spectroscopy to analyze nutrient stress-related changes in biomass composition of phytoplankton algae. *Plant Physiol. Biochem.*, 43: 717–726.

32. Heraud, P., Stojkovic, S., Beardall, J., McNaughton, D., and Wood, B.R. (2008) Intercolonial variability in macromolecular composition in P-starved and P-replete *Scenedesmus* populations revealed by infrared microspectroscopy. *J. Phycol.*, 44: 1335–1339.

33. Sigee, D.C., Dean, A., Levado, E., and Tobin, M.J. (2002) Fourier-transform infrared spectroscopy of *Pediastrum*. *J. Phycol.*, 37: 19–26.

34. Liang, Y., Beardall, J., and Heraud, P. (2006) Changes in growth, chlorophyll fluorescence and fatty acid composition with culture age in batch cultures of *Phaeodactylum tricornutum* and *Chaetoceros muelleri* (Bacillariophyceae). *Bot. Mar.*, 49: 165–173.

35. Dean, A.P. and Sigee, D.C. (2006) Molecular heterogeneity in *Aphanizomenon flos-aquae* and *Anabaena flos-aquae* (Cyanophyta): A synchrotron-based Fourier-transform infrared study of lake micropopulations. *Eur. J. Phycol.*, 41: 201–212.

36. Borchardt, M.A. (1996) Nutrients. In *Algal Ecology: Freshwater Benthic Ecosystem*, Stevenson, R.J., Bothwell, M.L., and Lowe, R.L., Eds. Academic Press: San Diego, pp. 184–228.

37. Murdock, J.N. and Wetzel, D.L. Nitrogen variability and uptake measurement in benthic diatoms with synchrotron infrared microspectroscopy. In press.

38. Toole, G.A., Kacurakova, M., Smith, A.C., Waldron, K.W., and Wilson, R.H. (2004) FT-IR study of the *Chara corallina* cell wall under deformation. *Carbohydr. Res.*, 339: 629–635.

39. Dunn, E.K., Shoue, D.A., Huang, X., Kline, R.E., MacKay, A.L., Carpita, N.C., Taylor, I.E.P., and Mandoli, D.F. (2007) Spectroscopic and biochemical analysis of regions of the cell wall of the unicellular "Mannan weed," *Acetabularia acetabulum*. *Plant Cell Physiol.*, 48: 122–133.

40. Chiovitti, A., Heraud, P., Dugdale, T.M., Hodson, O.M., Curtain, R.C.A., Dagastine, R.R., Wood, B.R., and Wetherbee, R. (2008) Divalent cations stabilize the aggregation of sulfated glycoproteins in the adhesive nanofibers of the biofouling diatom *Toxarium undulatum*. *Soft Matter*, 4: 811–820.

41. Lin, R. and Ritz, G.P. (1993) Reflectance FT-IR microspectroscopy of fossil algae contained in organic-rich shales. *Appl. Spectros.*, 47: 265–271.

42. Kansiz, M., Heraud, P., Wood, B., Burden, F., Beardall, J., and McNaughton, D. (1999) Fourier transform infrared microspectroscopy and chemometrics as a tool for the discrimination of cyanobacterial strains. *Phytochemistry*, 52: 407–417.

43. Heraud, P., Wood, B.R., Tobin, M.J., Beardall, J., and McNaughton, D. (2005) Mapping of nutrient-induced biochemical changes in living algal cells using synchrotron infrared microspectroscopy. *FEMS Microbiol. Lett.*, 249: 219–225.

44. Sigee, D.C., Bahram, F., Estrada, B., Webster, R.E., and Dean, A.P. (2007) The influence of phosphorus availability on carbon allocation and P quota in *Scenedesmus subspicatus*: A synchrotron-based FTIR analysis. *Phycologia*, 46: 583–592.

45. Dean, A.P., Estrada, B., Nicholson, J.M., and Sigee, D.C. (2008) Molecular response of *Anabaena flos-aquae* to differing concentrations of phosphorus: A combined Fourier transform infrared and X-ray microanalytical study. *Phycol. Res.*, 56: 193–201.

46. Yee, N., Benning, L.G., Phoenix, V.R., and Ferris, F.G. (2004) Characterization of metal-cyanobacteria sorption reactions: A combined macroscopic and infrared spectroscopic investigation. *Environ. Sci. Techn.*, 38: 775–782.

47. Patel, S.A., Currie, F., Thakker, N., and Goodacre, R. (2008) Spatial metabolic fingerprinting using FT-IR spectroscopy: Investigating abiotic stresses on *Micrasterias hardyi*. *Analyst*, 133: 1707–1713.